

Article

Combined Effect of Buoyancy Force and Navier Slip on Entropy Generation in a Vertical Porous Channel

Adetayo Samuel Egunjobi * and Oluwole Daniel Makinde

Institute for Advance Research in Mathematical Modelling and Computation, Cape Peninsula University of Technology, P.O. Box 1906, Bellville 7535, South Africa;
E-Mail: makinded@cput.ac.za

* Author to whom correspondence should be addressed; E-Mail: samdet1@yahoo.com;
Tel.: +26-48-1635-6585.

Received: 18 May 2012; in revised form: 2 June 2012 / Accepted: 2 June 2012 /

Published: 12 June 2012

Abstract: In this paper, we investigate the combined effects of buoyancy force and Navier slip on the entropy generation rate in a vertical porous channel with wall suction/injection. The nonlinear model problem is tackled numerically using Runge–Kutta–Fehlberg method with shooting technique. Both the velocity and temperature profiles are obtained and utilized to compute the entropy generation number. The effects of slip parameter, Brinkmann number, the Peclet number and suction/injection Reynolds number on the fluid velocity, temperature profile, Nusselt number, entropy generation rate and Bejan number are depicted graphically and discussed quantitatively.

Keywords: buoyancy force; Navier slip; porous channel; suction/injection; entropy generation; irreversibility

PACS Codes: 44.10.+a; 47.11.-j; 47.15.gm

Nomenclature

V	dimensional velocity, [ms^{-1}]	u	fluid velocity, [ms^{-1}]
P	fluid pressure, [Nm^{-2}]	x,y	cartesian coordinates, [m]
T	fluid temperature, [K]	g	acceleration due to gravity, [ms^{-2}]
E_G	volumetric rate of entropy production, [$\text{W/m}^3 \text{K}$]	w	dimensionless velocity

T_0	temperature at $y = 0$, [K]	T_h	temperature at $y = h$, [K]
c_p	specific heat at constant pressure, [J/kgK]	Re	Reynolds number, [-]
Pe	Peclet number, [-]	Br	Brinkman number
C_f	skin friction, [-]	N_u	Nusselt number, [-]
N_1	entropy generation due to heat transfer	N_1	entropy generation due to viscous dissipation
Be	Bejan number, [-]	K	pressure gradient

Greek Letters

μ	fluid viscosity, [Nsm ⁻²]	α	thermal diffusivity, [m ² s ⁻¹]
γ_1, γ_2	slip coefficients, [m]	β	volumetric expansion coefficient, [K ⁻¹]
ρ	fluid density, [kgm ⁻³]	θ	dimensionless temperature, [-]
β_1, β_2	dimensionless slip coefficients, [-]	Ω	dimensionless temperature difference, [-]
ϕ	irreversibility ratio, [-]		

1. Introduction

The study of fluid flow and heat transfer in a porous channel have received considerable attention during the last several decades due to their relevance in a wide range of biological and engineering settings such as ground water hydrology, irrigation, and drainage problems and also in absorption and filtration processes in chemical engineering. The scientific treatment of the problems of irrigation, soil erosion and tile drainage are the present focus of the development of porous media flow [1–3]. Meanwhile, the problem of the slip flow regime is very important in this era of modern science, technology and vast ranging industrialization. In many practical applications, the fluid adjacent to a solid surface no longer takes the velocity of the surface. The fluid at the surface has a finite tangential velocity; it slips along the surface. The flow regime is called the slip flow regime and its effect cannot be neglected. The effects of slip conditions on the hydromagnetic steady flow in a channel with permeable boundaries were discussed by Makinde and Osalusi [4]. Khalid and Vafai [5] obtained the closed form solutions for steady periodic and transient velocity field under slip condition. Watanebe *et al.* [6] studied the effect of Navier Slip on Newtonian fluids at solid boundary. Chen and Tian [7] investigated entropy generation in a micro annulus flow and discussed the influence of velocity slip on entropy generation. Chauhan and Kumar [8] investigated fully developed forced convection in a circular channel filled with a highly porous medium saturated with a rarefied gas and uniform heat flux at the wall in the slip-flow region, using the Darcy extended Brinkman–Forchheimer momentum equation and the entropy generation due to heat transfer. Meanwhile, there is continuous transfer of momentum and energy between the fluid and the solid boundaries, causing the fluid to undergo irreversible processes and therefore increase the entropy generation in the system. Since entropy production destroys the available energy in the system, the improvement in the energy utilization during the fluid convection is one of the fundamental problems in engineering processes. The optimal use of energy can be achieved, if the second law of thermodynamics is taken into consideration. Mahmud and Fraser [9] examined the flow, thermal and entropy generation fields inside a parallel-plate porous channel, when subjected to differentially heated isothermal wall. Chauhan and

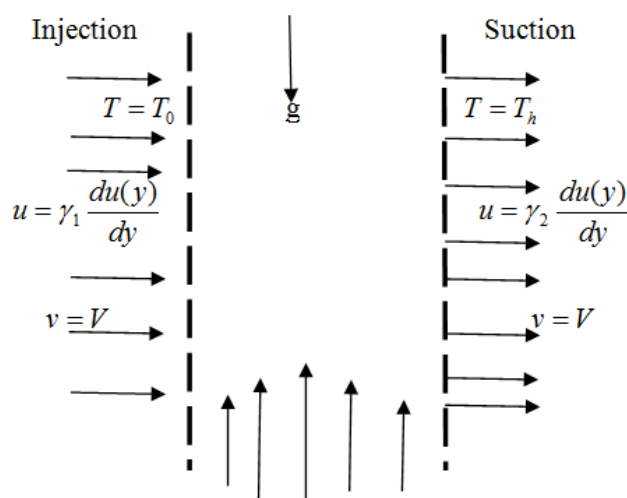
Olkha [10] investigated the hydrodynamics and heat transfer of the flow of a third-grade fluid incorporating entropy analysis. Chauhan and Kumar [11] analyzed the heat transfer and entropy generation in a situation where the compressible fluid flow is caused by moving an impermeable wall of a composite channel partially filled with a porous medium and a clear fluid. Chauhan and Rastogi [12] considered an unsteady two-dimensional MHD flow and heat transfer through a porous medium adjacent to a non-isothermal stretching sheet. Several researchers have carried out analysis on second law analysis such as [13–16]. Furthermore, starting from the pioneering work of Bejan [17–18], several investigations on entropy generation on fluid flow under various physical situations have been done [19–30]. Chen [31] performed a detailed study on the effects of Reynolds number and Grashof number on entropy generation inside disk driven convective flow for the first time. Chen *et al.* [32] investigated the effects of Rayleigh number, curvature of annulus and Prandtl number on the flow pattern, temperature distribution and entropy generation for natural convection inside a vertically concentric annular space. It appears that very little or no study has considered the combined effects of buoyancy force and velocity slip on the entropy generation in a porous channel with suction and injection, which is the focus of this paper.

In this paper, the inherent irreversibility of a porous channel under the influence of velocity slip and buoyancy force is investigated numerically using Runge–Kutta–Fehlberg method with shooting technique. The solution of the resulting momentum and energy balance equations are reported for representative values of thermo-physical parameters characterizing the fluid convection processes.

2. Mathematical Analysis

The steady laminar incompressible viscous boundary layer flow through a vertical porous channel with non-uniform temperature, injection at the left wall and suction at the right wall under the combined effect of buoyancy forces and Navier slip as shown in Figure 1 below are considered.

Figure 1. Flow configuration and coordinate system.



The density variation due to buoyancy effects is taken into account in the momentum equation using Boussinesq approximation. The momentum and energy equations describing the flow can be written as:

Momentum equation:

$$V \frac{du(y)}{dy} = -\frac{1}{\rho} \frac{dP}{dx} + \frac{\mu}{\rho} \frac{d^2u(y)}{dy^2} + g\beta(T - T_0) \quad (1)$$

Energy equation:

$$V \frac{dT(y)}{dy} = \alpha \frac{d^2T(y)}{dy^2} + \frac{\mu}{\rho c_p} \left(\frac{du(y)}{dy} \right)^2 \quad (2)$$

with the boundary conditions:

$$\begin{aligned} v(0) = V, \quad u(0) = \gamma_1 \frac{du(0)}{dy}, \quad T(0) = T_0 \\ v(h) = V, \quad u(h) = \gamma_2 \frac{du(h)}{dy}, \quad T(h) = T_h \end{aligned} \quad (3)$$

where u is the velocity of the fluid, P is the fluid pressure, μ is the fluid viscosity, α is the thermal diffusivity, ρ is the fluid density, c_p is the specific heat at constant pressure, T is the temperature, γ_1 and γ_2 are slip coefficients, β is volumetric expansion coefficient and g is acceleration due to gravity. The authors introduced the following dimensionless quantities:

$$\theta = \frac{T - T_0}{T_h - T_0}, \quad K = -\frac{d\bar{P}}{dx}, \quad \bar{x} = \frac{x}{h}, \quad \bar{P} = \frac{Ph}{\mu V}, \quad w = \frac{u}{V}, \quad \eta = \frac{y}{h} \quad (4)$$

Substituting Equation (4) into Equations (1)–(3), the authors obtained:

$$\frac{d^2w(\eta)}{d\eta^2} - \text{Re} \frac{dw(\eta)}{d\eta} + K + Gr\theta(\eta) = 0 \quad (5)$$

$$\frac{d^2\theta(\eta)}{d\eta^2} - \text{Pe} \frac{d\theta(\eta)}{d\eta} + Br \left(\frac{dw(\eta)}{d\eta} \right)^2 = 0 \quad (6)$$

with the boundary conditions:

$$w(0) = \beta_1 \frac{dw(0)}{d\eta}, \quad \theta(0) = 0 \quad (7)$$

$$w(1) = \beta_2 \frac{dw(1)}{d\eta}, \quad \theta(1) = 1 \quad (8)$$

where:

$$\text{Re} = \frac{V \rho h}{\mu} \quad (\text{Reynolds number}),$$

$$\text{Pe} = \frac{V h}{\alpha} \quad (\text{Peclet number}),$$

$$K = -\frac{d\bar{P}}{dx} \quad (\text{Pressure gradient parameter}),$$

$$Br = \frac{V^2 \mu}{\rho c_p \alpha (T_h - T_0)} \text{ (Brinkman number),}$$

$$Gr = \frac{g \beta \rho h^2 (T_h - T_0)}{\mu V} \text{ (Grashof number),}$$

$$\beta_1 = \frac{\gamma_1}{h} \text{ (Slip parameter),}$$

$$\beta_2 = \frac{\gamma_2}{h} \text{ (Slip parameter).}$$

Equations (5)–(6) together with boundary conditions (7)–(8) are coupled nonlinear boundary value problems which are solved numerically using Runge–Kutta–Fehlberg method with shooting technique. The numerical solution procedure employed to solve the model boundary valued problem in Equations (5)–(8) is based on shooting techniques [20,33]. It involves, transforming Equations (5)–(8) into a set of initial value problems. The transformed initial value problems will contain few unknown initial values that need to be determined. After guessing the unknown initial values, a fourth order Runge–Kutta iteration scheme is employed to integrate the set of initial valued problems until the given boundary conditions are satisfied. The computations are done by a written program which used a symbolic and computational computer language MAPLE. The entire procedure is implemented on MAPLE. The gradient of the velocity at the channel walls referring to skin friction is equivalent to:

$$S_f = \mu \left. \frac{du}{dy} \right|_{y=0,h} \quad (9)$$

therefore, the skin-friction coefficient at the wall using dimensionless quantities (4) is given by:

$$C_f = \frac{h}{V \mu} = \left. \frac{dw(\eta)}{d\eta} \right|_{\eta=0,1} \quad (10)$$

The rate of heat transfer at the channels wall in dimensionless form is given by:

$$N_u = - \left. \frac{d\theta(\eta)}{d\eta} \right|_{\eta=0,1} \quad (11)$$

3. Entropy Generation

The convection process along a porous channel is naturally irreversible. Exchange of energy and momentum within the fluid and at the solid boundaries causes non-equilibrium condition, which therefore leads to continuous entropy generation in the porous channel. Bejan [9] gave volumetric rate of entropy generation in a Cartesian coordinates as:

$$E_G = \frac{k}{T_0^2} \left(\left(\frac{dT}{dx} \right)^2 + \left(\frac{dT}{dy} \right)^2 \right) + \frac{\mu}{T_0} \left(2 \left\{ \left(\frac{du}{dx} \right)^2 + \left(\frac{dv}{dy} \right)^2 \right\} + \left(\frac{du}{dy} + \frac{dv}{dx} \right)^2 \right) \quad (12)$$

The velocity and temperature distributions are simplified in many fundamental convection problems by assuming that the flow is fully developed by [1] as:

$$E_G = \frac{k}{T_0^2} \left(\frac{dT}{dy} \right)^2 + \frac{\mu}{T_0} \left(\frac{du}{dy} \right)^2 \quad (13)$$

where the first term on the right hand side of Equation (13) is the irreversibility due to heat transfer and the second term is the entropy generation due to viscous dissipation. Introducing the dimensionless quantities defined in (4) to Equation (13), the authors obtained:

$$N_s = \frac{T_0^2 h^2 E_G}{k(T_h - T_0)^2} = \left(\frac{d\theta(\eta)}{d\eta} \right)^2 + \frac{Br}{\Omega} \left(\frac{dw(\eta)}{d\eta} \right)^2 \quad (14)$$

where $\Omega = (T_h - T_0)/T_0$ is the temperature difference parameter and:

$$N_1 = \left(\frac{d\theta(\eta)}{d\eta} \right)^2, N_2 = \frac{Br}{\Omega} \left(\frac{dw(\eta)}{d\eta} \right)^2 \quad (15)$$

where N_1 represents irreversibility due to heat transfer and N_2 gives entropy generation due to viscous dissipation. In order to have an idea whether the entropy generation due to viscous dissipation dominates over the irreversibility due to heat transfer or *vice versa*, the authors defined irreversibility ratio as:

$$\phi = \frac{N_2}{N_1} \quad (16)$$

Entropy generation due to viscous dissipation dominates if $\phi > 1$ and if $0 \leq \phi < 1$, then irreversibility due to heat transfer dominates, but if $\phi = 1$ implies that both of them contribute equally.

The Bejan number (Be) is defined as:

$$Be = \frac{N_1}{N_s} = \frac{1}{1 + \phi} \quad (17)$$

where $Be = 1$ is the limit at which heat transfer irreversibility dominates, $Be = 0$ is the limit at which fluid friction irreversibility dominates, and $Be = 1/2$ implies that both of them contribute equally.

4. Results and Discussion

The validity of boundary layer approximation for this model channel flow problem can be attributed to the fact that the combined effects of suction and injection on the flow system are more pronounced within the channel walls region [9,20]. Using appropriate parameters, the detailed discussion and graphical representation of the results of above equations are reported in this section. We refer to vertical lines at $\eta = 0$ as injection wall and at $\eta = 1$ as suction wall in this discussion. Figure 2 depicts the velocity profile while Grashof number (Gr) is increasing and other parameters remain constant. The buoyancy effect on the flow system is demonstrated by variation in parameter value of Grashof number (Gr). The choice of the values for Gr used in this paper is motivated by the increasing effects of buoyancy due to gravity and temperature difference between the channel walls. Increase in Gr, decreased the fluid injection toward the channel from the injection wall and increased the suction fluid rate at the suction wall. Consequently, the velocity increased at the injection wall and decreased at the suction wall. A reversal flow is noticed at the suction wall as Gr is increasing. Towards the centerline

of the channel, the flow attains its maximum velocity and it is asymmetric. Figure 3 shows the effect of increasing Reynolds number (Re). As Re is increasing, fluid injection into the channel, as well as the fluid suction rate is increasing. At the injection wall, the velocity decreases and the flow reversal at the suction wall increases.

Figure 2. Velocity Profile, $Re = 2$, $Br = 1$, $K = \beta_1 = \beta_2 = 0.1$, $Pe = 3$.

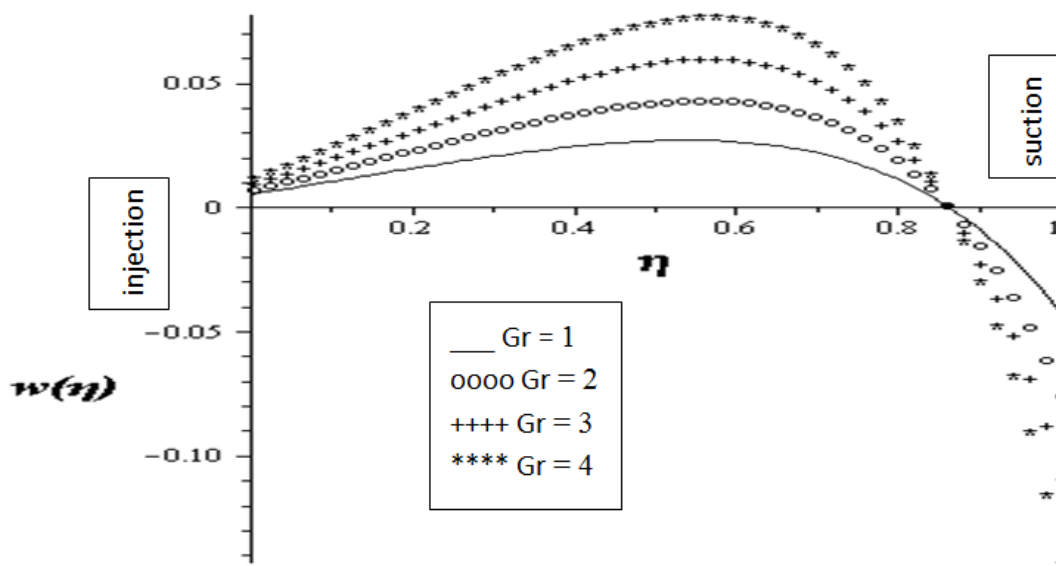


Figure 3. Velocity Profile, $Gr = Br = 1$, $K = \beta_1 = \beta_2 = 0.1$, $Pe = 3$.

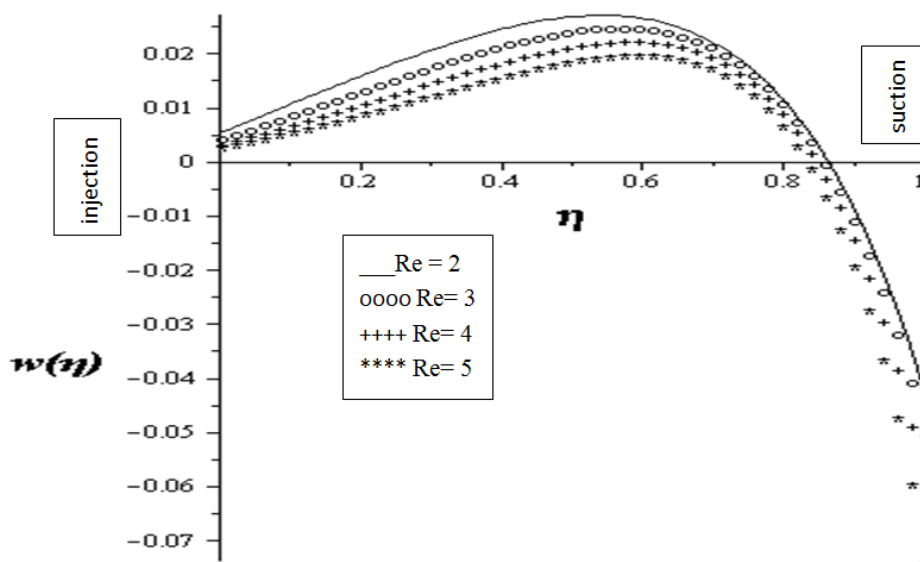


Figure 4 depicts the velocity profile while the pressure gradient (K) is increasing. As the pressure gradient is increasing, there is a little increase in velocity at the injection wall and a reversal flow at the suction wall is noticed. The flow attains its maximum velocity very close to the centerline of the channel. Figure 5 shows the velocity profile as Peclet number (Pe) is increasing. As Pe is increasing, the fluid injection into the channel at the injection wall increases, similarly, there is an increase in the

fluid suction rate at the suction wall. The velocity at injection wall decreases a little but at suction wall, the velocity increases. Meanwhile, at the centerline of the channel, the velocity decreases greatly.

Figure 4. Velocity Profile, $Gr = Br = 1, Re = 2, \beta_1 = \beta_2 = 0.1, Pe = 3$.

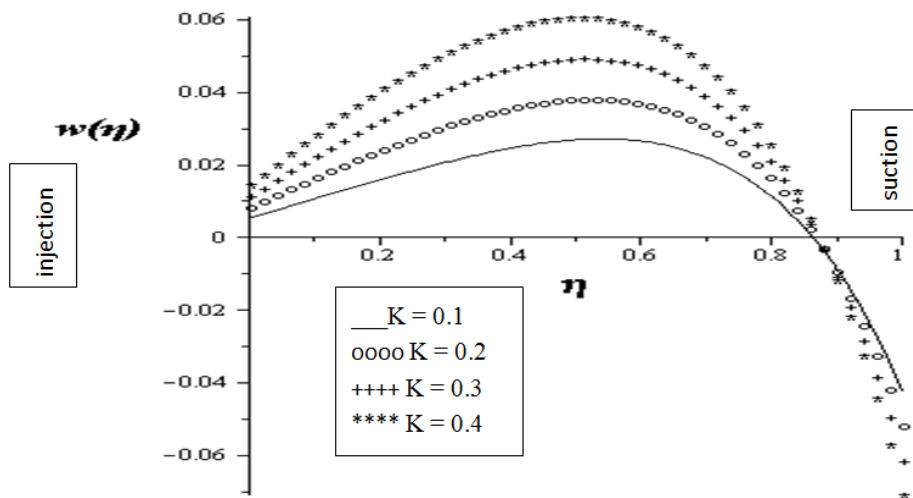


Figure 5. Velocity Profile, $Gr = Br = 1, Re = 2, \beta_1 = \beta_2 = 0.1, K = 0.1$.

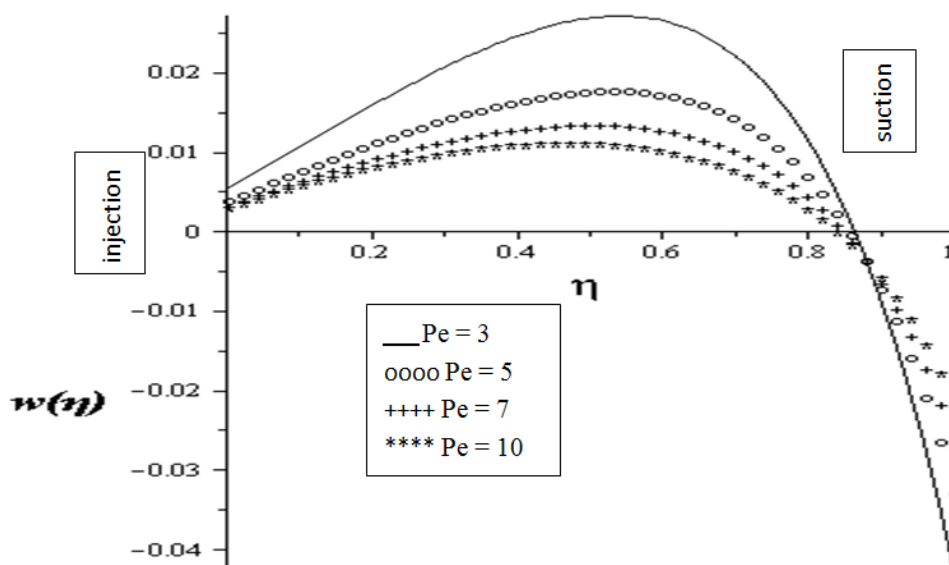


Figure 6 shows the velocity profile with increase in slip parameter (β_1). As β_1 is increasing, the flow velocity at the injection wall increases and a slight reversal flow effect at the suction wall is noticed. Figure 7 depicts an increase in slip parameter (β_2). As β_2 is increasing, the flow velocity at the injection wall decrease slightly but greater decrease in the velocity is noticed at the suction wall.

Figure 6. Velocity Profile, $Gr = Br = 1$, $Re = 2$, $\beta_2 = 0.1$, $K = 0.1$, $Pe = 3$.

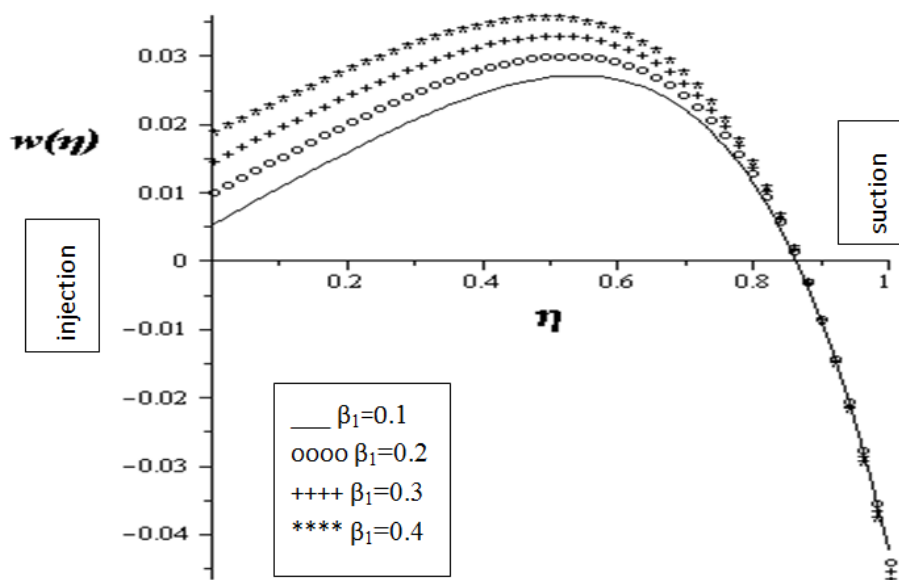
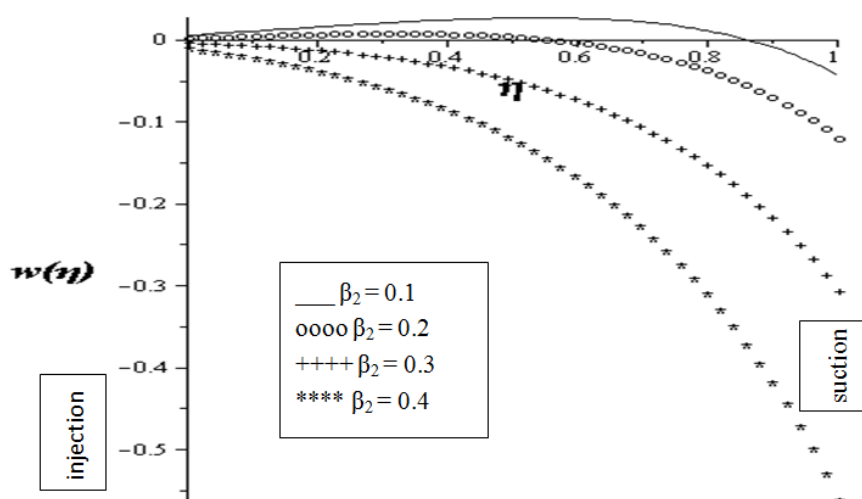


Figure 7. Velocity Profile, $Gr = Br = 1$, $Re = 3$, $\beta_1 = 0.1$, $K = 0.1$, $Pe = 3$.



When each of the parameters (Gr , Re , Br , K , β_1 , β_2) varies while others remain constant for the temperature profile, there is no effect on both suction and injection channel walls. Figure 8 depicts the temperature profile as Peclet Number (Pr) is increasing. An increase in the Peclet number leads to a decrease in the temperature at both injection and suction channel walls.

Figure 9 depicts the variation of Peclet number and its effect on entropy generation number. The graph reveals that as the Peclet number is increasing, entropy generation number has no effect on the injection wall but rather on the suction wall, with great increase in entropy generation. This shows that there are restrictive medium leading to high disorder in the fluid particle at the suction wall.

Figure 8. Temperature Profile, $Gr = Br = 1, Re = 2, \beta_1 = \beta_2 = 0.1, K = 0.1$.

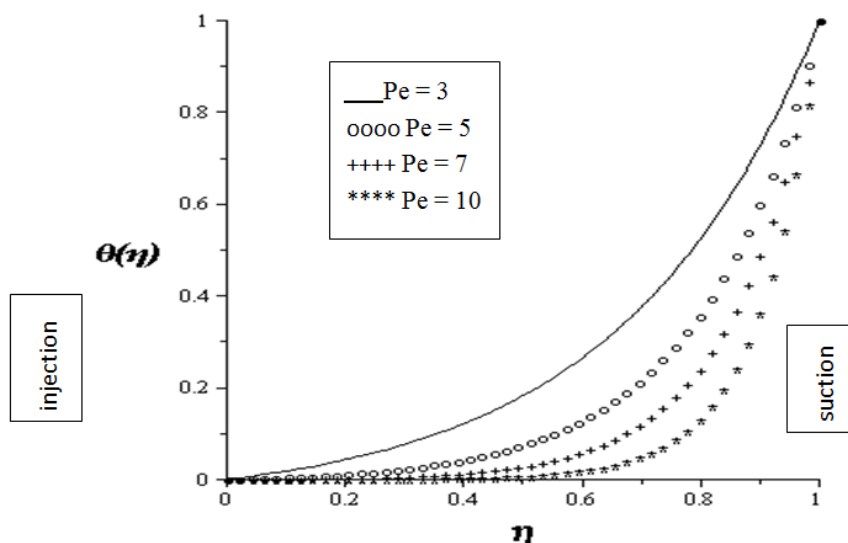
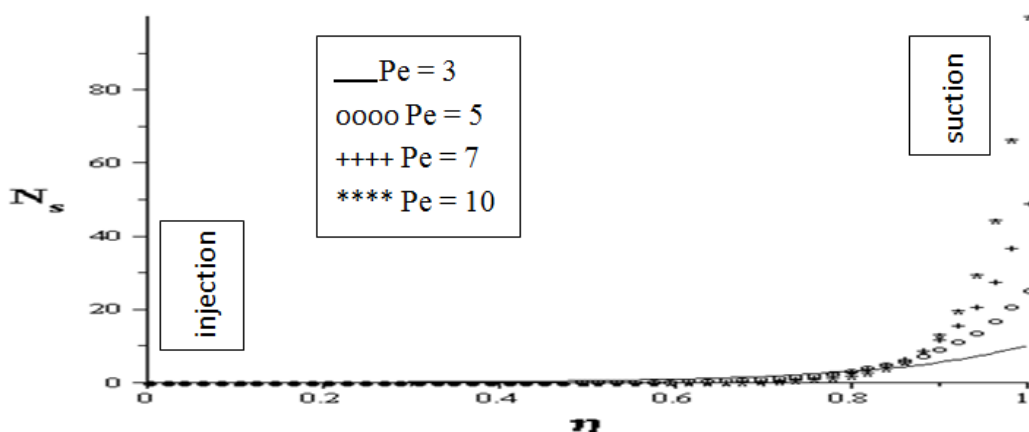


Figure 9. Entropy generation profile, $Gr = 1, Re = 2, k = 0.1, Br = 1, \beta_1 = \beta_2 = 0.1, \Omega = 1$.



Figures 10 and 11 depict an increase in group parameter ($Br\Omega^{-1}$) and Grashof number (Gr) and their effects on entropy generation. As $Br\Omega^{-1}$ and (Gr) are increasing in Figure 10 and Figure 11 respectively, a slight increase in entropy generation on the injection wall and greater increase in entropy generation on the suction wall are noticed. This indicates that, there is little restrictive medium at the injection walls and more restrictive medium at the suction walls. Like Figures 10 and 11, Figure 12 holds the same explanation as the pressure gradient parameter K varies. Figure 13 takes into consideration the variation of the asymmetric slip parameter β_1 and its effect on entropy generation. This means that there is less restrictive medium at the injection wall but more restrictive medium at the suction wall. Figure 14 depicts variation in slip parameter β_2 . As β_2 increased, there is an increase in entropy generation on both walls but with a greater increase on the suction wall.

Figure 10. Entropy generation profile, $Gr = 1$, $Re = 2$, $k = 0.1$, $Pe = 0.1$, $\beta_1 = \beta_2 = 0.1$.

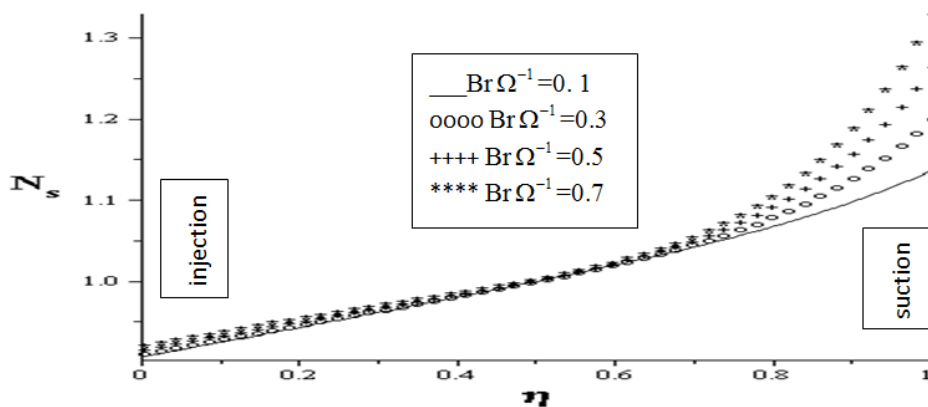


Figure 11. Entropy generation profile, $\Omega = 1$, $Pe = 0.1$, $Re = 2$, $K = 0.1$, $Br = 1$, $\beta_1 = \beta_2 = 0.1$.

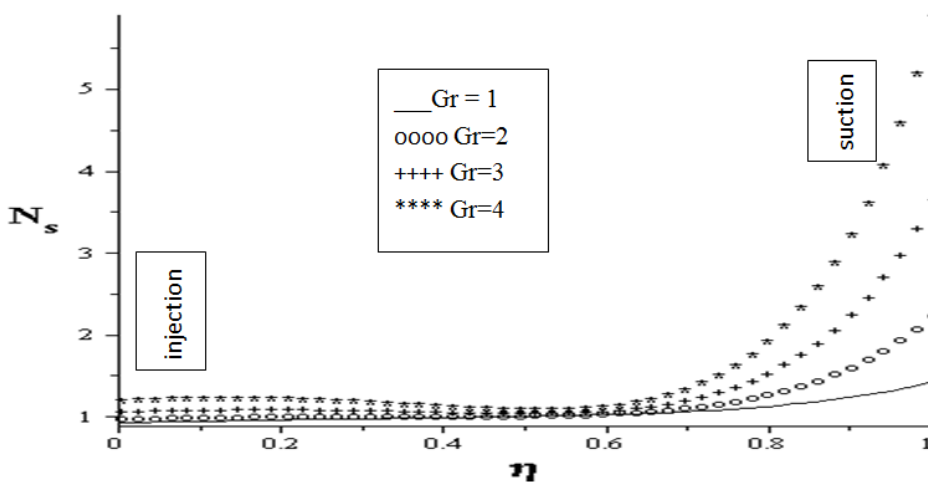


Figure 12. Entropy generation profile, $Gr = 1$, $Re = 2$, $Br = 1$, $Pe = 3$, $\beta_1 = \beta_2 = 0.1$, $\Omega = 1$.

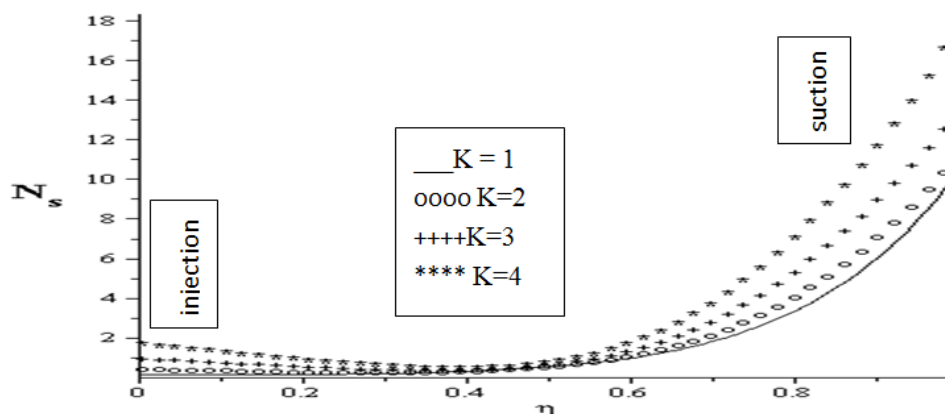


Figure 13. Entropy generation profile, $Pe = 0.95, Re = 2, K = 0.1, Br = 1, \beta_2 = 0.1, \Omega = 1, Gr = 4.$

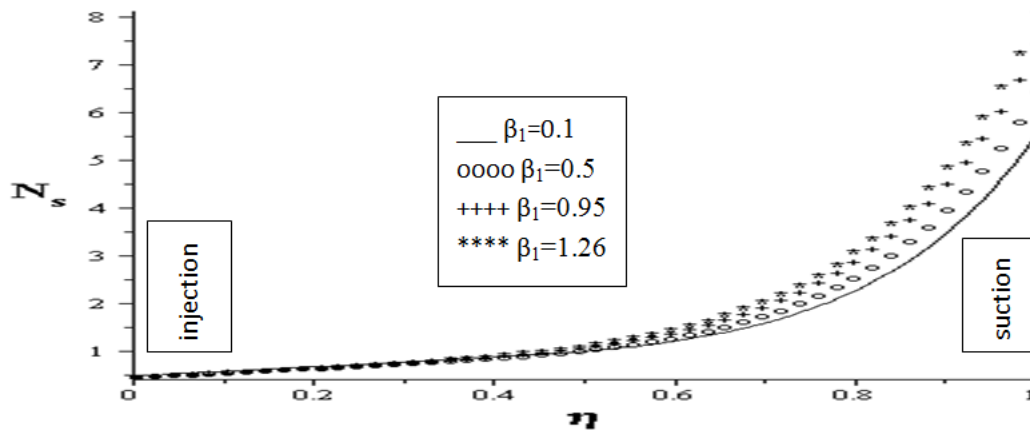
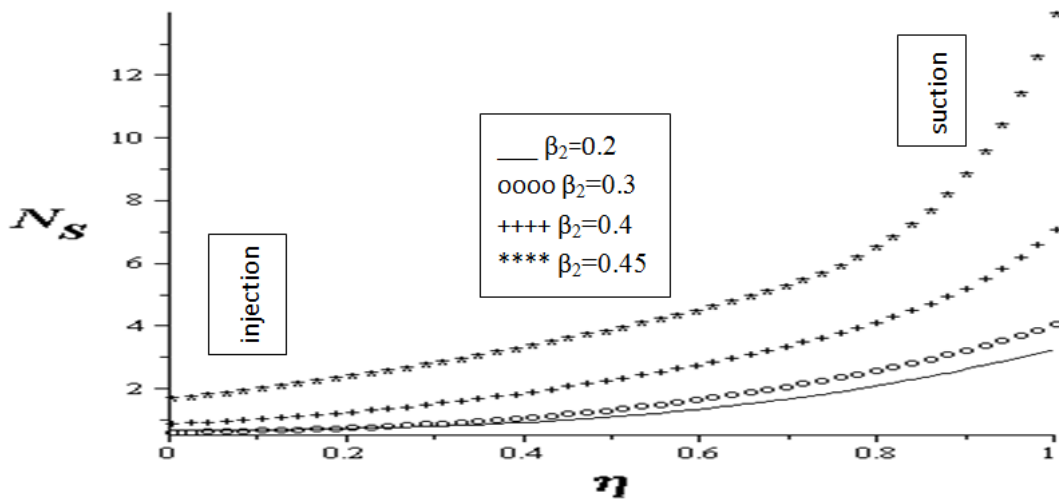


Figure 14. Entropy generation profile, $Re = 2, Pe = 3, K = 0.1, Br = 1, \beta_1 = 0.1, \Omega = 1, Gr = 2.$



Figures 15–20 show the effect of Reynolds number, Peclet number, slip parameters, group parameters, pressure gradient and Grashof number on the Bejan number. Figure 15 takes into account the variation of Reynolds number and its effect on the Bejan number. The graph shows that as Reynolds number is increasing, Bejan number on the injection wall is increasing while Bejan number on suction wall is decreasing. Hence, irreversibility due to heat transfer dominates the flow process at the injection wall and irreversibility due to fluid friction dominates at the suction wall. Figure 16 considers the variation of the pressure gradient parameter (K) and its effect on Bejan number. As pressure gradient parameter is increasing, a decrease in the Bejan number at both walls is noticed. Hence, irreversibility due to fluid friction dominates at both walls. At the centerline of the channel, both irreversibility due to heat transfer and irreversibility due to fluid friction contribute equally. Figure 17 looks at increase in Peclet number and its effect on Bejan number. As the Peclet number is increasing, Bejan number at the injection wall is decreasing and increasing at suction wall. Therefore, irreversibility due to fluid friction dominates the injection channel wall and irreversibility due to heat transfer dominates the flow process at the suction wall, but both of them contributed equally at the centerline of the channel. Figure 18 takes into account the variations of group parameters and its effect on Bejan number. The graph shows that as the group parameter is increasing, at the injection and

suction channel walls, Bejan number is decreasing. This implies that irreversibility due to heat transfer decrease at both walls, but at the centerline of the channel both irreversibility due to fluid friction and irreversibility due to heat transfer contributed equally.

Figure 15. Bejan Number profile, $Pe = 3$, $Gr = Br\Omega^{-1} = 1$, $K = \beta_1 = \beta_2 = 0.1$.

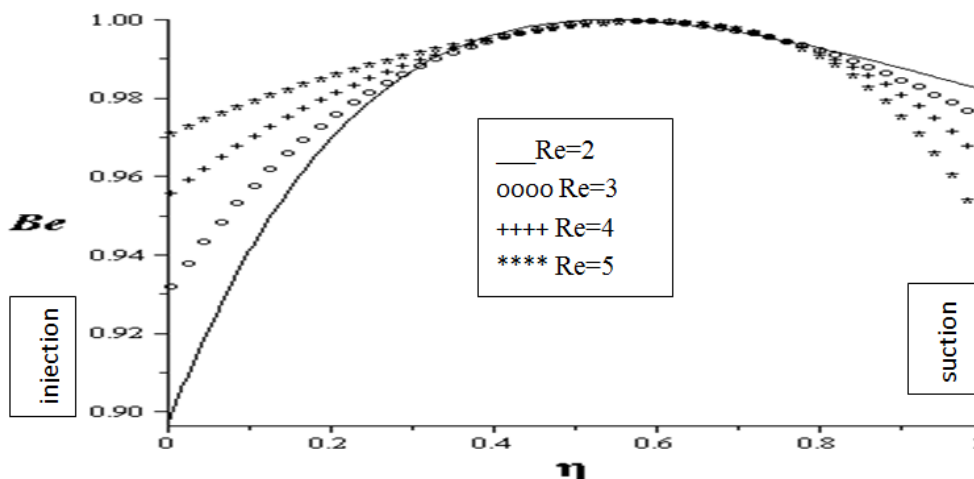


Figure 16. Bejan Number profile, $Re = 2$, $Gr = Br\Omega^{-1} = 1$, $\beta_1 = \beta_2 = 0.1$, $Pe = 3$.

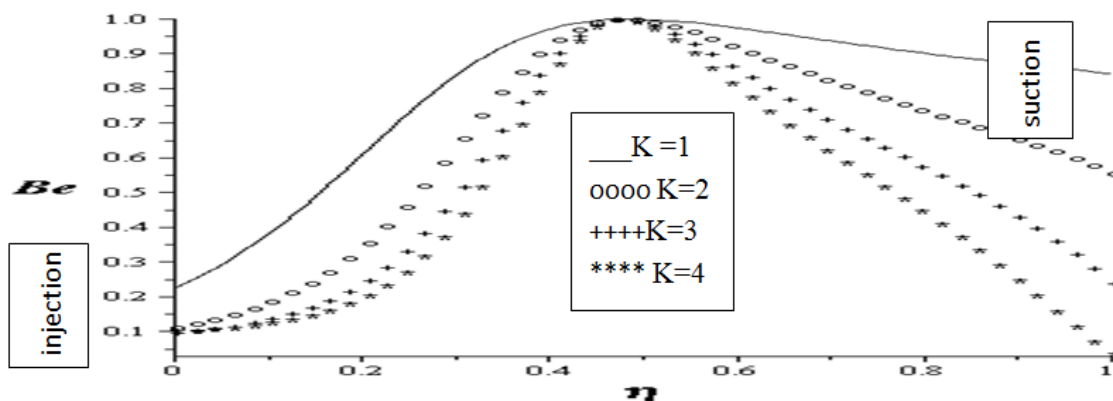


Figure 17. Bejan Number profile, $Re = 2$, $Gr = K = Br\Omega^{-1} = 1$, $\beta_1 = \beta_2 = 0.1$.

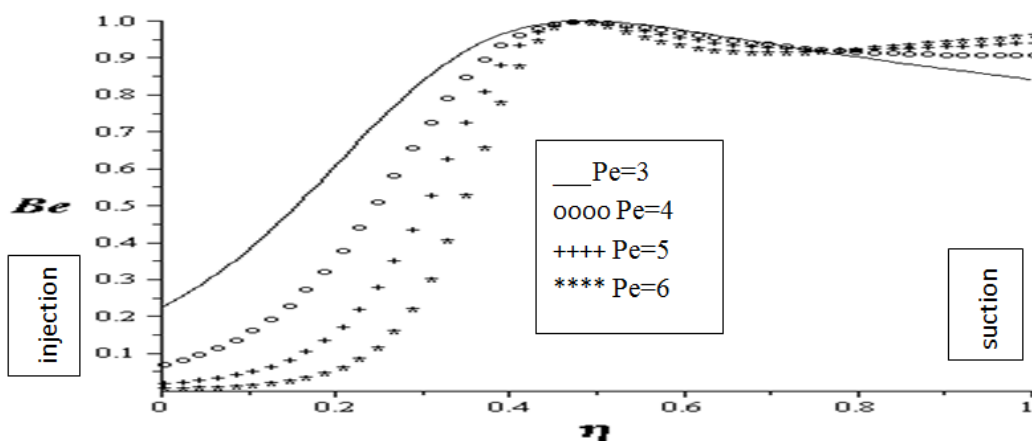
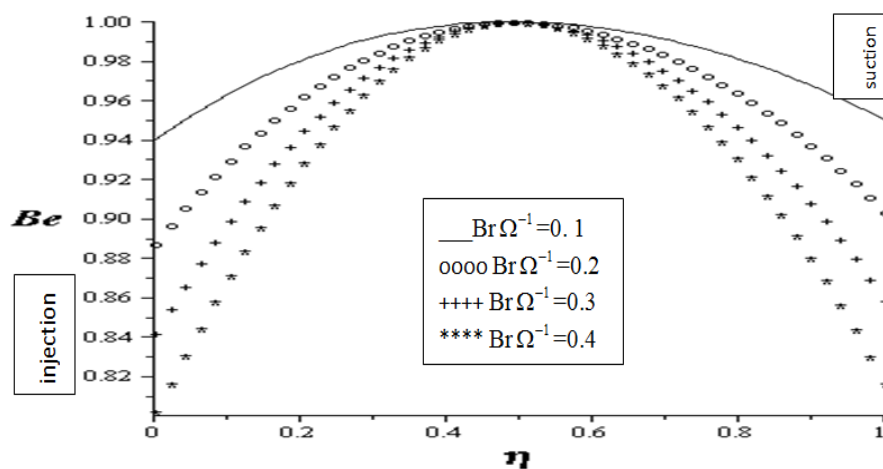


Figure 18. Bejan Number profile, $Re = 2$, $Gr = K = 1$, $\beta_1 = \beta_2 = 0.1$, $Pe = 1.5$.



Figures 19 and 20 show increase in the asymmetric slip coefficients β_1 and β_2 with their effects on Bejan number. The graphs show that as asymmetric slip coefficients β_1 and β_2 are increasing; Bejan number is decreasing at injection wall and increasing at suction wall. A flow reversal at suction wall is noticed as well.

Figure 19. Bejan Number profile, $Re = 2$, $Gr = K = Br\Omega^{-1} = 1$, $\beta_2 = 0.1$, $Pe = 2$.

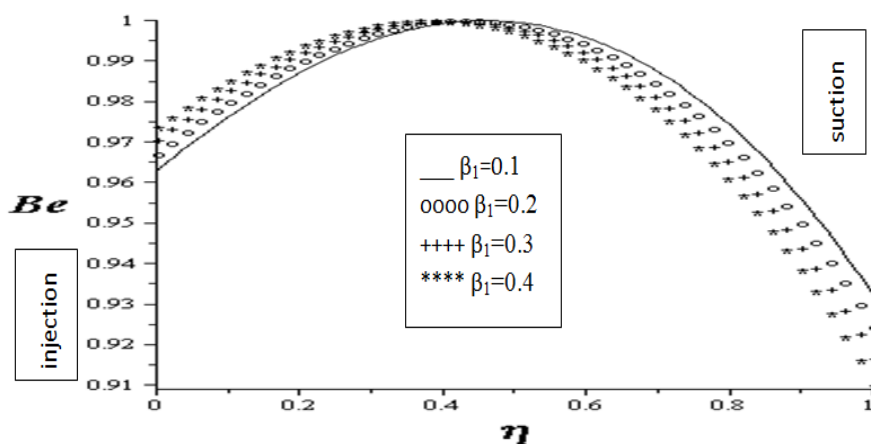
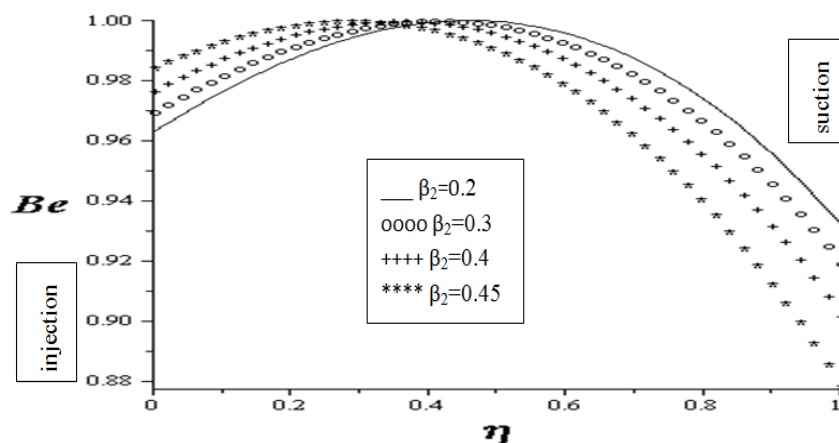


Figure 20. Bejan Number profile, $Re = 2$, $Gr = K = 1$, $\beta_1 = Br\Omega^{-1} = 0.1$, $Pe = 0.71$.



5. Conclusions

The combined effect of buoyancy forces and Navier slip on the entropy generation rate in a vertical porous channel with wall suction/injection was investigated. In the course of considering the effect of buoyancy forces (*i.e.*, increases in Grashof number), the authors noticed a slight increase in the entropy generation rate at the injection wall and sporadic increase at the suction wall. Furthermore, entropy generation decreased at the injection wall and increased at the suction wall as slip parameter β_1 increased. However, as the slip parameter β_2 increased, the entropy generation rate at both suction and injection walls increased. Also, increase in both slip parameters (β_1 and β_2) resulted in a flow reversal in the Bejan number.

References

1. White, F.S. *Viscous Fluid Flow*; McGraw-Hill: New York, NY, USA, 1974.
2. Ingham, D.B.; Pop, I. *Transport Phenomena in Porous Media*; Pergamon: Oxford, UK, 2002.
3. Nield, D.A.; Bejan, A. *Convection in Porous Media*, 3rd ed.; Springer: New York, NY, USA, 2006.
4. Makinde, O.D.; Osalusi, E. MHD steady flow in a channel with slip at the permeable boundaries. *Rom. J. Phys.* **2006**, *51*, 319–328.
5. Khaled, A.R.A.; Vafai, K. The effect of the slip condition on stokes and couette flows due to an oscillatory wall: Exact solutions. *Int. J. Non. Lin. Mech.* **2004**, *39*, 795–809.
6. Watanebe, K.; Yanuar, M.H. Slip of Newtonian fluids at solid boundary. *J. Jpn. Soc. Mech. Eng.* **1998**, *B41*, 525.
7. Chen, S; Tian, Z. Entropy generation analysis of thermal micro-Couette flows in slip regime. *Int. J. Therm. Sci.* **2010**, *49*, 2211–2221.
8. Chauhan, D.S.; Kumar, V. Effects of slip conditions on forced convection and entropy generation in a circular channel occupied by a highly porous medium: Darcy extended Brinkman-Forchheimer model. *Turk. J. Eng. Environ. Sci.* **2009**, *33*, 91–104.
9. Mahmud, S.; Fraser, R.A. Flow, thermal and entropy generation characteristic inside a porous channel with viscous dissipation. *Int. J. Therm. Sci.* **2005**, *44*, 21–32.
10. Chauhan, D.S.; Olkha, A. Entropy generation and heat transfer effects on non-Newtonian fluid flow in annular pipe with natural permeable boundaries. *Int. J. Energ. Tech.* **2011**, *3*, 1–19.
11. Chauhan, D.S.; Kumar, V. Heat transfer and entropy generation during compressible fluid flow in a channel partially filled with porous medium. *Int. J. Energ. Tech.* **2011**, *3*, 1–10.
12. Chauhan, D.S.; Rastogi, P. Heat transfer and entropy generation in MHD flow through a porous medium past a stretching sheet. *Int. J. Energ. Tech.* **2011**, *3*, 1–13.
13. Hooman, K. Entropy-energy analysis of forced convection in a porous-saturated circular tube considering temperature-dependent viscosity effects. *Int. J. Exergy* **2006**, *3*, 436–451.
14. Hooman, K.; Gurgenci, H.; Merrikh, A.A. Heat transfer and entropy generation optimization of forced convection in a porous-saturated duct of rectangular cross-section. *Int. J. Heat Mass Tran.* **2007**, *50*, 2051–2059.

15. Tasnim, S.H.; Mahmud, S.; Mamun, M.A.H. Entropy generation in a porous channel with hydromagnetic effects. *Exergy* **2002**, *2*, 300–308.
16. Ozkol, I.; Komurgoz, G.; Arikoglu, A. Entropy generation in the laminar natural convection from a constant temperature vertical plate in an infinite fluid. *Proc. IME J. Power. Energ.* **2007**, *221*, 609–616.
17. Bejan, A. *Convection Heat Transfer*; John Wiley and Sons: New York, NY, USA, 1984.
18. Bejan, A. *Entropy generation minimization*; CRC Press: New York, NY, USA, 1996.
19. Makinde, O.D.; Osalusi, E. Second law analysis of laminar flow in a channel filled with saturated porous media. *Entropy* **2005**, *7*, 148–160.
20. Makinde, O.D. Second law analysis for variable viscosity hydromagnetic boundary layer flow with thermal radiation and Newtonian heating. *Entropy* **2011**, *13*, 1446–1464.
21. Mahmud, S.; Tasnim, S.H.; Mamun, H.A.A. Thermodynamics analysis of mixed convection in a channel with transverse hydromagnetic effect. *Int. J. Therm. Sci.* **2003**, *42*, 731–740.
22. Chen, S.; Tolke, J.; Krafczyk, M. Numerical investigation of double-diffusive (natural) convection in vertical annulus with opposing temperature and concentration gradients. *Int. J. Heat Fluid Flow* **2010**, *31*, 217–226.
23. Chen, S.; Du, R. Entropy generation of turbulent double-diffusive natural convection in a rectangle cavity. *Energy* **2011**, *36*, 1721–1734.
24. Chen, S. Entropy generation of double-diffusive convection in the presence of rotation. *Appl. Math. Comput.* **2011**, *217*, 8575–8597.
25. Chen, S.; Li, J.; Han, H.; Liu, Z.; Zheng, Z. Effects of hydrogen addition on entropy generation in ultra-lean counter-flow methane-air premixed combustion. *Int. J. Hydrogen Energ.* **2010**, *35*, 3891–3902.
26. Chen, S.; Mi, J.; Liu, H.; Zheng, C. First and second thermodynamic-law analyses of hydrogen-air counter-flow diffusion combustion in various combustion modes. *Int. J. Hydrogen Energ.* **2012**, *37*, 5234–5245.
27. Chen, S.; Zheng, C. Entropy generation in impinging flow confined by planar opposing jets. *Int. J. Therm. Sci.* **2010**, *49*, 2067–2075.
28. Chen, S.; Liu, Z.; Liu, J.; Li, J.; Wang, L.; Zhen, C. Analysis of entropy generation in hydrogen-enriched ultra-lean counter-flow methane-air non-premixed combustion. *Int. J. Hydrogen Energ.* **2010**, *35*, 12491–12501.
29. Chen, S.; Han, H.; Liu, Z.; Li, J.; Zheng, C. Analysis of entropy generation in non-premixed hydrogen versus heated air counter-flow combustion. *Int. J. Hydrogen Energ.* **2010**, *35*, 4736–4746.
30. Chen, S. Analysis of entropy generation in counter-flow premixed hydrogen-air combustion. *Int. J. Hydrogen Energ.* **2010**, *35*, 1401–1411.
31. Chen, S. Entropy generation inside disk driven rotating convective flow. *Int. J. Therm. Sci.* **2011**, *50*, 626–638.
32. Chen, S.; Liu, Z.; Bao, S.; Zheng, C. Natural convection and entropy generation in a vertically concentric. *Int. J. Therm. Sci.* **2010**, *49*, 2439–2452.

33. Nachtsheim, P. R.; Swigert, P. *Satisfaction of the Asymptotic Boundary Conditions in Numerical Solution of the System of Nonlinear Equations of Boundary Layer Type*. NASA TND-3004, 1965.

© 2012 by the authors; licensee MDPI, Basel, Switzerland. This article is an open access article distributed under the terms and conditions of the Creative Commons Attribution license (<http://creativecommons.org/licenses/by/3.0/>).